Article

Cell Reports

The Heterochronic Gene *lin-14* Controls Axonal Degeneration in *C. elegans* Neurons

Graphical Abstract

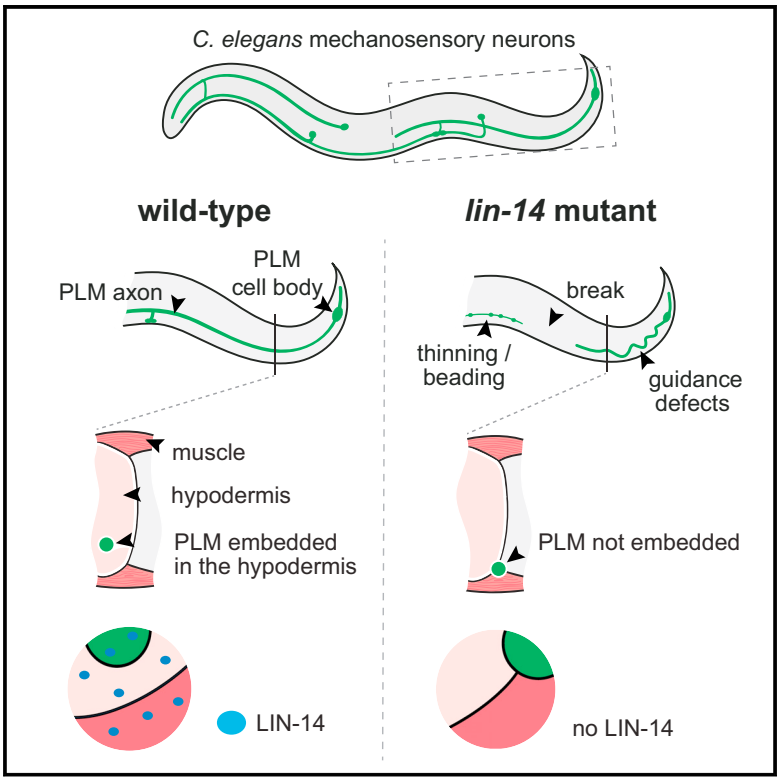

Highlights

- LIN-14 prevents axonal degeneration and maintains neuronal integrity
- LIN-14 functions early in development to prevent axonal degeneration later in life
- LIN-14 controls the position and embedment of the PLM axon in the epidermis
- *lin-14* mutants cause axonal damage through a two-hit effect

Authors

Fiona K. Ritchie, Rhianna Knable, Justin Chaplin, Rhiannon Gursanscky, Maria Gallegos, Brent Neumann, Massimo A. Hilliard

Correspondence

m.hilliard@uq.edu.au

In Brief

Maintenance of the long and thin axonal compartment is essential for neuronal function. Ritchie et al. found that LIN-14 is critical for maintaining neuronal integrity and preventing axonal degeneration. LIN-14 acts within the neuron as well as in the surrounding tissue to preserve the correct axonal position and structure.

Ritchie et al., 2017, Cell Reports *20*, 2955–2965
September 19, 2017
http://dx.doi.org/10.1016/j.celrep.2017.08.083

CellPress

Cell Reports
Article

The Heterochronic Gene *lin-14* Controls Axonal Degeneration in *C. elegans* Neurons

Fiona K. Ritchie,[1,4] Rhianna Knable,[1,4] Justin Chaplin,[1,4] Rhiannon Gursanscky,[1] Maria Gallegos,[2] Brent Neumann,[1,3] and Massimo A. Hilliard[1,5,*]
[1]Clem Jones Centre for Ageing Dementia Research, Queensland Brain Institute, The University of Queensland, Brisbane 4072, Australia
[2]Department of Biological Sciences, California State University East Bay, Hayward, CA 94542, USA
[3]Neuroscience Program, Monash Biomedicine Discovery Institute, and Department of Anatomy and Developmental Biology, Monash University, Melbourne, VIC 3800, Australia
[4]These authors contributed equally
[5]Lead Contact
*Correspondence: m.hilliard@uq.edu.au
http://dx.doi.org/10.1016/j.celrep.2017.08.083

SUMMARY

The disproportionate length of an axon makes its structural and functional maintenance a major task for a neuron. The heterochronic gene *lin-14* has previously been implicated in regulating the timing of key developmental events in the nematode *C. elegans*. Here, we report that LIN-14 is critical for maintaining neuronal integrity. Animals lacking *lin-14* display axonal degeneration and guidance errors in both sensory and motor neurons. We demonstrate that LIN-14 functions both cell autonomously within the neuron and non-cell autonomously in the surrounding tissue, and we show that interaction between the axon and its surrounding tissue is essential for the preservation of axonal structure. Furthermore, we demonstrate that *lin-14* expression is only required during a short period early in development in order to promote axonal maintenance throughout the animal's life. Our results identify a crucial role for LIN-14 in preventing axonal degeneration and in maintaining correct interaction between an axon and its surrounding tissue.

INTRODUCTION

Axonal degeneration is observed in a number of neurodegenerative diseases, including glaucoma and Alzheimer's, Parkinson's and motor neuron diseases (Cifuentes-Diaz et al., 2002; Fischer et al., 2005; Schlamp et al., 2006; Stokin et al., 2005; Trapp et al., 1998). In most cases, this is the initial event that correlates with disease onset and progression and can ultimately lead to death of the neuronal cell body (reviewed in Conforti et al., 2007; Raff et al., 2002). Remarkably, despite the critical importance of this biological process, we are only starting to understand the molecular elements and mechanisms that are in place to protect the axon (Coleman, 2005; Wang et al., 2012). In *C. elegans*, axonal degeneration can be initiated by mutations in the heat-shock transcription factor ortholog HSF-1 (Toth et al., 2012), by blocking mitochondrial transport into axons (Rawson et al., 2014), and by structural defects in the axon due to mutation of the α-tubulin acetyltransferase MEC-17, the α-tubulin MEC-12, the β-tubulin MEC-7 (Neumann and Hilliard, 2014), or the β-spectrin UNC-70 (Hammarlund et al., 2007).

LIN-14 is a transcription factor that is widely expressed in *C. elegans* and plays a key role in the heterochronic control of developmental events (Ambros and Horvitz, 1984, 1987). The expression of LIN-14 forms a steep temporal gradient during early development (Ruvkun and Giusto, 1989), with protein levels decreasing rapidly after the first larval (L1) stage due to suppression caused by the microRNA *lin-4* binding to a conserved region in the 3′ UTR of *lin-14* (Wightman et al., 1991, 1993). This change in expression during development is important for many of the functions of LIN-14 as a heterochronic timer. LIN-14 acts in a number of capacities in the nematode, including in the regulation of developmental timing in the lateral hypodermal cell lineages (Ambros and Horvitz, 1987) and in the control of lifespan by downregulating the activity of the insulin/IGF (insulin growth factor)-1 like signaling (IIS) pathway (Hristova et al., 2005). It has also been shown to have a number of functions in neurons, including directing cell-fate decisions in Q cell neuroblasts (Mitani et al., 1993), the precursors of the mechanosensory neurons anterior ventral microtubule neuron (AVM) and posterior ventral microtubule neuron (PVM). LIN-14 directs the timing of synaptic remodeling in GABAergic motor neurons (Hallam and Jin, 1998) and is a temporal regulator of axon guidance in the AVM and PVM neurons (Zou et al., 2012), and in the PVT interneuron (Aurelio et al., 2003).

Here, we identify a role for LIN-14 in preventing axonal degeneration. Animals carrying mutations in *lin-14* display a spontaneous and progressive axonal degeneration phenotype in the posterior lateral microtubule neuron (PLM) and the GABAergic motor neurons. We show that LIN-14 has cell-autonomous as well as non-cell-autonomous functions in these neurons and regulates the position and embedment of the axon within its surrounding tissue (the epidermis, also known as the hypodermis). This close interaction between the axon and its surrounding tissue is essential for maintenance of the axonal structure. We demonstrate that the timing of *lin-14* expression, early in the L1 stage, is critical for its protective function later in life. Finally, we reveal functional synergy in axonal protection between LIN-14 and the dual-leucine zipper kinase MAPKKK (mitogen-activated protein kinase kinase kinase) DLK-1.

RESULTS AND DISCUSSION

LIN-14 Is Necessary to Protect Axons from Degenerating

In wild-type *C. elegans*, the bipolar PLM neurons extend a short posterior neurite toward the tail of the animal and a long anterior axon that terminates in the mid-body section (Chalfie et al., 1985). A short branch extends ventrally from the axon, reaching the ventral nerve cord where it synapses with other neurons (Figures 1A and 1B). In wild-type animals, the axonal structure of this neuron is maintained over the lifespan of the animal, with aging inflicting ectopic branching, spines, and blebs, but very rarely breaks (Pan et al., 2011; Tank et al., 2011; Toth et al., 2012). We used the PLM axon as an experimental system in which to identify and study the molecular elements necessary to protect the axon. A serendipitous observation made while investigating axonal elongation revealed that animals carrying mutations in the gene *lin-14* (temperature-sensitive alleles *n179* and *n355n679* and the severe loss-of-function alleles *536n540* and *ma135*) presented axonal degeneration

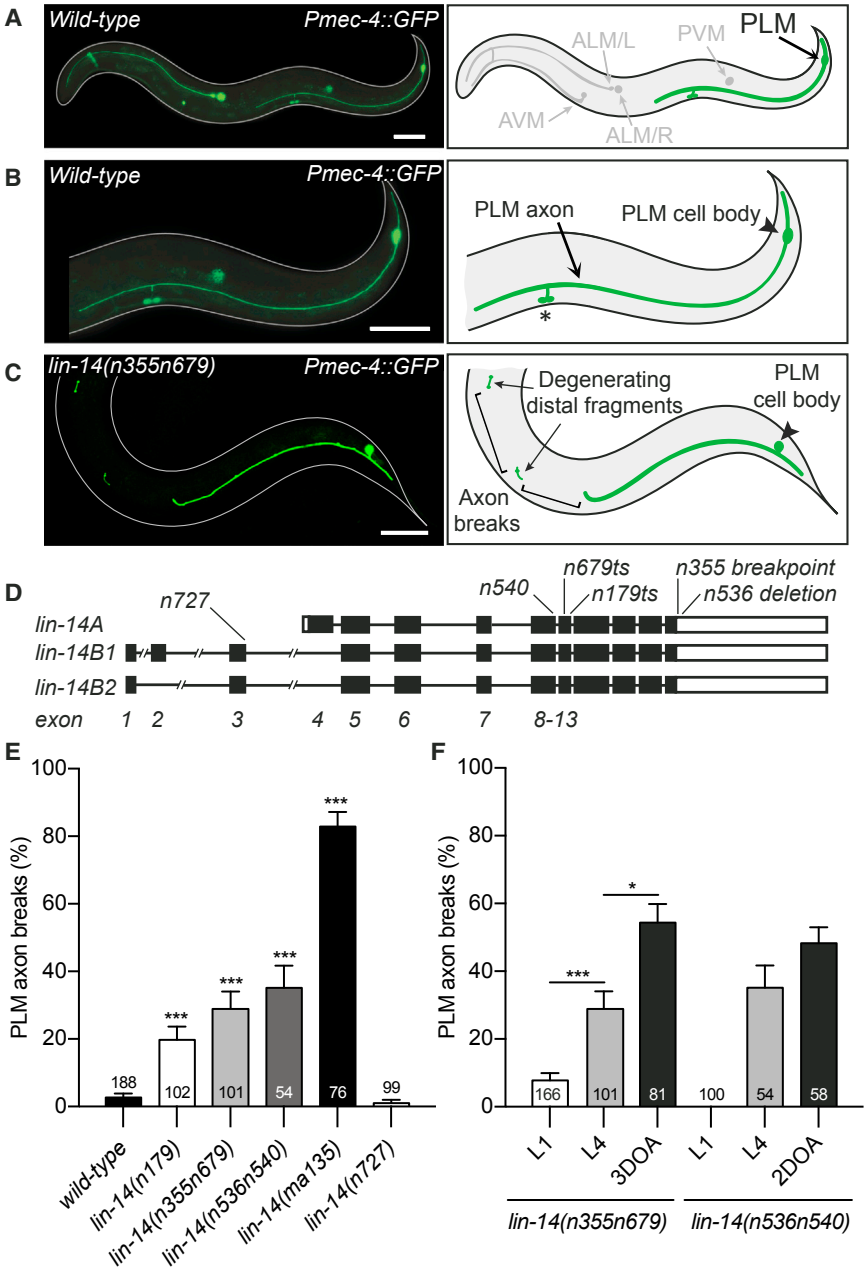

Figure 1. LIN-14 Prevents Axonal Degeneration

(A) Image and schematic of a wild-type *zdIs5 (Pmec-4::GFP)* larval stage four (L4) animal, illustrating the six mechanosensory neurons (PLM L/R, PVM, ALM L/R, and AVM). Anterior is left and ventral is down in this and all subsequent images.

(B) Image and schematic of a typical intact PLM neuron from an L4 wild-type animal. The cell body of PLM (arrowhead) is located on the posterior side of the animal's body and extends an anterior axon (arrow) that runs in the lateral cord. A ventral branch (asterisk) containing presynaptic sites extends to enter the ventral nerve cord.

(C) Image and schematic of typical axon breaks (bracketed regions) in an L4 *lin-14(n355n679)* mutant animal.

(D) Alternate splicing of the first four exons of *lin-14* result in three different LIN-14 protein isoforms (designated A, B1, and B2). The locations of key *lin-14* mutations are noted (the details of the *ma135* allele are not curated); exons are indicated with black boxes, introns are indicated with black lines, and UTRs are indicated with white boxes (adapted from Reinhart and Ruvkun, 2001).

(E) Axon breaks quantified in five different loss-of-function alleles of *lin-14*. *n179*, *n355n679*, *n536n540*, and *ma135* alleles affect both the LIN-14A and LIN14B isoforms and show a significant increase in the penetrance of PLM axon breaks, compared to the wild-type control. The *n727* allele in the region of *lin-14* specific to the B isoform has no effect. All experiments were performed at 25°C, except for those with alleles *n536n540* and *ma135*, which were performed at 23°C due to the strains not being able to withstand cultivation at the higher temperature.

(F) The axonal breaks and degeneration of PLM observed in *lin-14* mutants are progressive in nature and were tested in two alleles (*n355n679* and *n536n540*). No defects are present at hatching (data not shown); however, by mid-L1 stage, a small percentage of animals begin to display the defect. By the L4 stage, there is a highly significant increase in the penetrance of breaks, which continues to progress into adulthood; the *n536n540* animals were scored at the 2-day-old-adult (2DOA) stage, as they did not survive at 3DOA.

Scale bars, 50 μm; error bars represent SE of proportion; n values are indicated at the base of each graph. *p < 0.05; ***p < 0.001, from ANOVA and Dunnett's multiple comparison test for (E) (compared to wild-type) and Sidak's multiple comparison for (F).

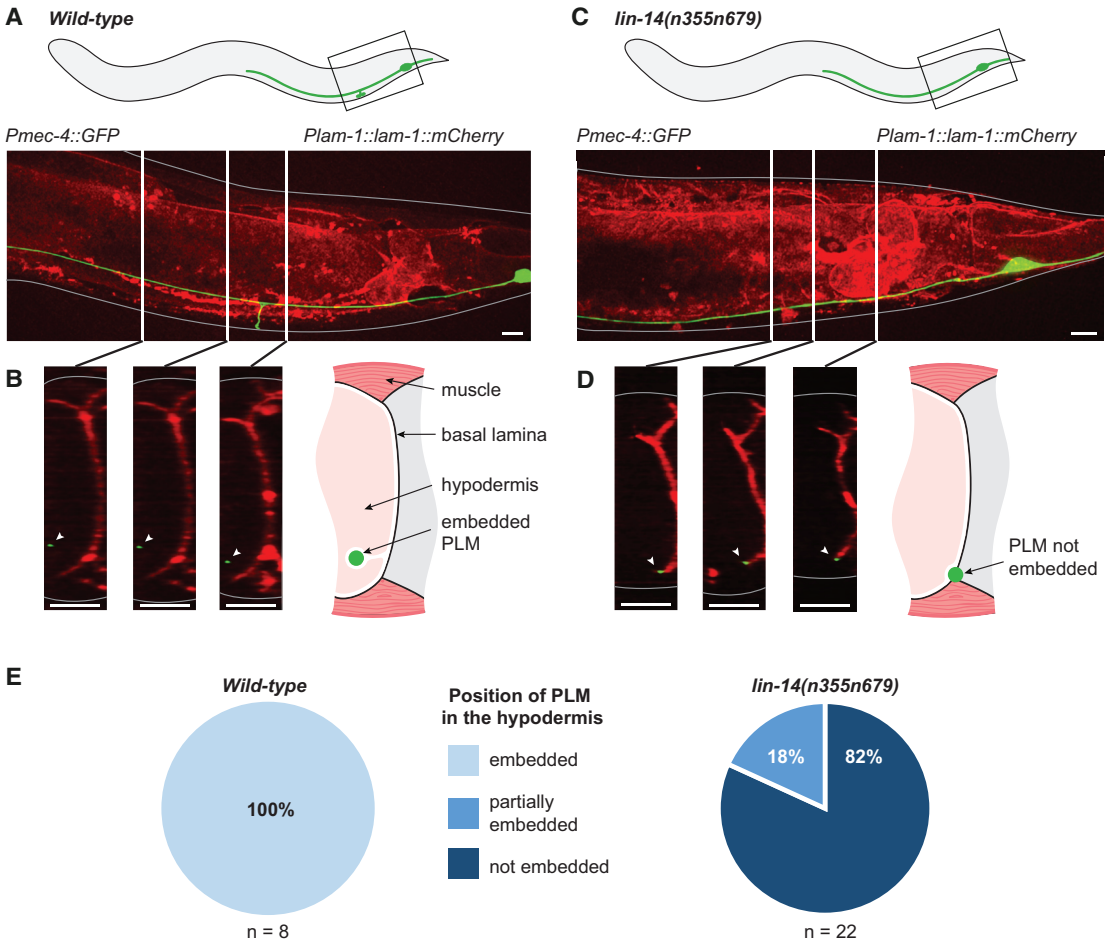

Figure 2. LIN-14 Is Required for Embedment of the PLM Axon

(A) Maximum-projection image and schematic of a wild-type *zdIs5(Pmec-4::GFP); qyIs127(Plam-1::lam-1::mCherry)* L4 animal, illustrating PLM (green) and the basal lamina (red).

(B) Representative YZ-plane cross-sections and schematic of a wild-type *zdIs5(Pmec-4::GFP); qyIs127(Plam-1::lam-1::mCherry)* L4 animal. This image demonstrates the position of the PLM axon (green) in relation to the basal lamina (red), with the PLM neuron appearing to be embedded in the hypodermis.

(C) Maximum-projection image and schematic of a *lin-14(n355n679)* L4 mutant animal in a *zdIs5(Pmec-4::GFP); qyIs127(Plam-1::lam-1::mCherry)* background.

(D) Representative YZ-plane cross-sections and schematic of a *lin-14(n355n679)* L4 mutant animal in a *zdIs5(Pmec-4::GFP); qyIs127(Plam-1::lam-1::mCherry)* background. This image demonstrates the position of the PLM axon (green) in relation to the basal lamina (red), with the PLM neuron appearing to be located on the border between the muscle and hypodermis.

(E) Quantification of the embedment defect in *lin-14(n355n679)* mutant animals compared to wild-type animals. Each axon was imaged for approximately 75 μm starting from the cell body, and every z stack analyzed along its entire length. Animals were scored as "embedded" if the axon appeared to be embedded for its entire section, "partially embedded" if only some regions of the axon were embedded, and "not embedded" if no embedment could be visualized.

Scale bars, 5 μm.

phenotypes characterized by breaks in the PLM axon, visible as interruptions of GFP along the axonal tract (Figures 1C–1E). In addition, *lin-14* mutant animals displayed a range of other defects, including axonal thinning and beading, aberrant axonal branching and guidance (in the form of axonal sagging/remodeling), and loss of the synaptic branch (Figure S1). A similar pattern of defects was also found in the GABAergic motor neurons of *lin-14* mutant animals (Figures S2A–S2D), suggesting a more general role for this molecule across the nervous system in conferring protection from axonal degeneration.

Three different splicing isoforms have been described for *lin-14*: LIN-14A, -B1 and -B2 (Figure 1D) (Reinhart and Ruvkun, 2001; Wightman et al., 1991). Previous studies have shown that the LIN-14A isoform alone is sufficient for functionality in a variety of contexts (Hallam and Jin, 1998; Hong et al., 2000). To determine whether this is also the case for PLM axonal protection, we examined an existing mutation that is specific to the B isoforms (*n727*). In *lin-14(n727)* animals, a single-nucleotide transition is present in exon three, resulting in a missense mutation that exclusively affects the differentially spliced B isoforms. These animals did not present any differences in axon

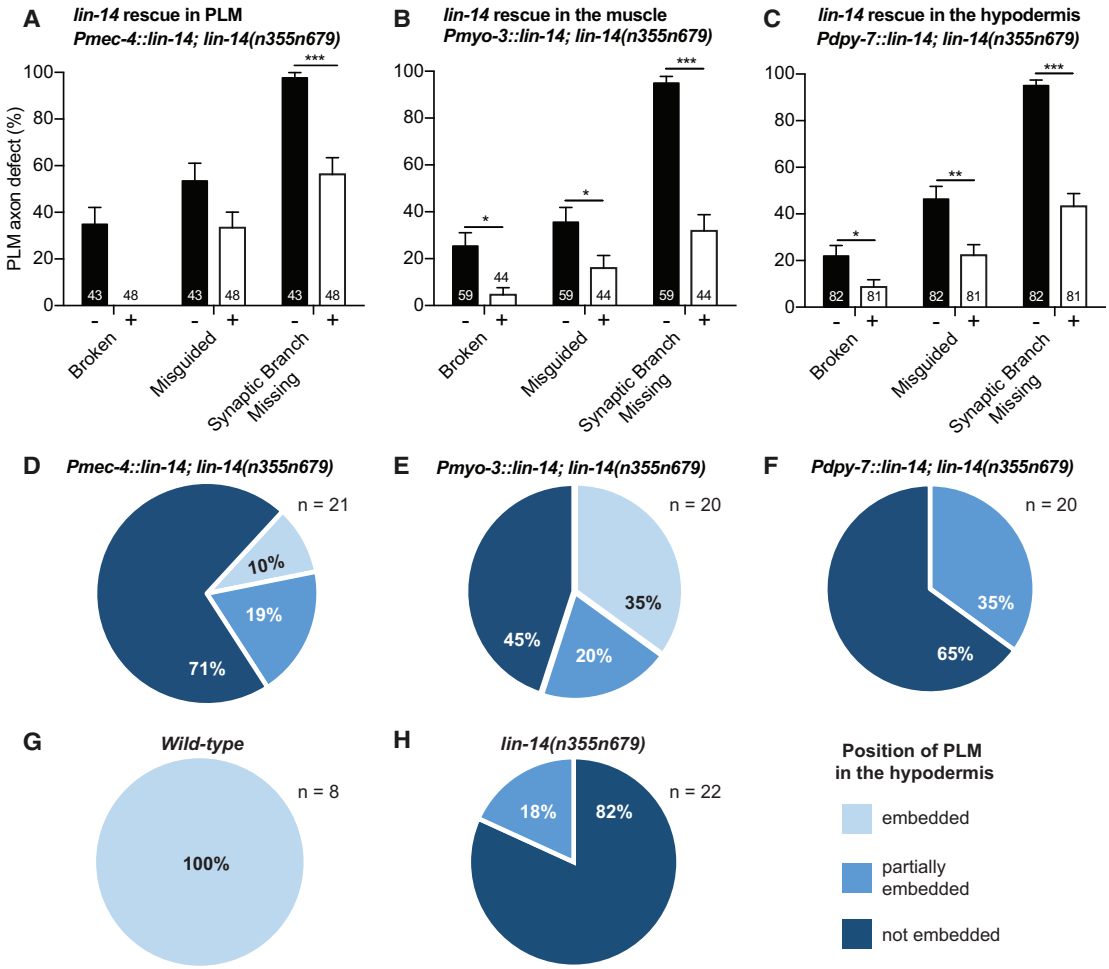

Figure 3. LIN-14 Acts Both Cell Autonomously and Non-cell Autonomously in Preventing Axonal Degeneration and Synaptic Branch Formation

(A) *lin-14(n355n679)* mutants carrying the *Pmec-4::lin-14* transgene (+) present rescue in the penetrance of breaks and synaptic branch formation but do not rescue axon guidance, compared to their non-transgenic siblings (-), indicating a cell-autonomous function of LIN-14 in protecting the PLM axon from degeneration and synaptic branch formation within the neuron.

(B) *lin-14(n355n679)* mutants carrying the *Pmyo-3::lin-14* transgene (+) present rescue in the penetrance of breaks, synapse branch formation, and axon guidance, compared to their non-transgenic siblings (-), indicating a non-cell-autonomous function of LIN-14 in protecting the PLM axon from degeneration, axon guidance, and synaptic branch formation within the muscle.

(C) *lin-14(n355n679)* mutants carrying the *Pdpy-7::lin-14* transgene (+) present rescue in the penetrance of breaks, synapse branch formation, and axon guidance, compared to their non-transgenic siblings (-), indicating a non-cell-autonomous function of LIN-14 in protecting the PLM axon from degeneration, axon guidance, and synaptic branch formation within the hypodermis.

(D–H) Each axon was imaged for approximately 75 μm starting from the cell body, and every z stack analyzed along its entire length. Animals were scored as "embedded" if the axon appeared to be embedded for its entire section, "partially embedded" if only some regions of the axon were embedded, and "not embedded" if no embedment could be visualized. While in all three rescue lines — specifically in (D) PLM neurons (*Pmec-4::lin-14*), (E) body wall muscles (*Pmyo-3::lin-14*), and (F) hypodermal cells (*Pdpy-7::lin-14*) — there is an improvement in the embedment defect, it is most notable when *lin-14* is rescued in the muscle. Data for (G) wild-type and (H) *lin-14* mutants are the same as reported in Figure 2E.

Error bars represent SE of proportion; n values are indicated at the base of each graph or adjacent to each pie chart. *$p < 0.05$; **$p < 0.01$; ***$p < 0.001$, from t test.

morphology compared to the wild-type control animals (strain *zdIs5(Pmec-4::GFP)*) (Figure 1E), suggesting that the LIN-14A isoform is sufficient for maintaining axonal integrity.

PLM is born during embryogenesis, and by hatching, its axon has nearly reached its final destination near the mid-body of the animal (Gallegos and Bargmann, 2004). To determine the onset of axonal degeneration in *lin-14* mutants, we analyzed animals at different developmental stages, including in the L1 stage (after hatching), in the fourth and final larval stage (L4), and in adults. Consistent with a progressive axonal degeneration defect, we found that the PLM axon developed normally and was intact at hatching. However, by the L4 stage and into adulthood, it had become highly defective (Figure 1F). To analyze *lin-14*-mediated axonal degeneration in closer detail, time-lapse imaging of

individual animals was performed from larval stage 3 (L3) to adulthood (Figure S3). Defects first appeared as thinning of the axon (Figure S3A). This was followed by the development of guidance defects (Figure S3B) and, subsequently, clear breaks appearing along the axon (Figure S3C). The breaks occurred in the same region of the neuron as where the thinning and guidance defects initially appeared, suggesting that these phenotypes are a precursor to axonal degeneration. The damaged section directly surrounding the break was then cleared away. Axon guidance defects alone, however, were not sufficient to cause axonal degeneration. This was determined by quantifying axonal breaks in the known axonal guidance mutants *unc-53* and *dgn-1* (Hekimi and Kershaw, 1993; Johnson and Kramer, 2012). Animals carrying the *unc-53(e2432)* mutation had a 27.4% (±5.7%, SE of proportion) penetrance of PLM axonal guidance defects and no axonal breaks (n = 62); *dgn-1(cg121)* mutants had 44.1% (±3.9%, SE of proportion) PLM axonal guidance defects and only 1.5% (±1.5%, SE of proportion) penetrance of axonal breaks (n = 68).

LIN-14 Controls the Position and Embedment of the PLM Axon in the Hypodermis

During normal development, the PLM axon begins adjacent to the muscle before becoming embedded in the hypodermis as development progresses beyond the L1 stage (Emtage et al., 2004). The worsening and variety of axonal phenotypes observed in *lin-14* mutants led us to investigate whether the PLM axonal positioning and embedment in the hypodermis were affected. By labeling the basal lamina (using a *Plam-1::lam-1::mCherry* transgene), we used confocal optical cross-sections to examine the position of the axon in relation to the hypodermis. For all analyses conducted, a representative image of approximately 75 μm of the axon from the cell body was taken to quantify the embedment. In wild-type L4 animals, PLM was embedded within the hypodermis along the entire section analyzed (Figures 2A, 2B, and 2E). In contrast, the hypodermis failed to fully embed the PLM axon in *lin-14(n355n679)* L4 animals (Figures 2C–2E). In more than 80% of the *lin-14* mutants, the PLM axon was absent from the hypodermis (not embedded), whereas in the remaining animals, only some regions were embedded (partially embedded) (Figures 2C and 2D). Thus, in the absence of LIN-14, PLM axons do not become surrounded by the hypodermis and, without this supporting structure, are unable to be maintained over the animal's lifetime. These results highlight the importance of the surrounding tissue in preserving the integrity of the axon and suggest that they play an active role in maintaining the structure of the PLM axon.

The expression pattern of *lin-14* has previously been characterized and includes expression in the hypodermis, muscles, intestine, and neurons (Hong et al., 2000). To determine the expression of LIN-14 specifically within PLM, we used a transgenic strain carrying a GFP-tagged version of LIN-14 driven by the endogenous promoter, as well as a cytoplasmic red fluorescent protein (RFP) driven by the *mec-4* promoter (visible in PLM); we found that LIN-14 was, indeed, present in the PLM nucleus (Figure S4).

LIN-14 could, in principle, exert its function directly in PLM in a cell-autonomous fashion, through other surrounding cells in a non-cell-autonomous manner, or through a combination of both. To address this issue, we generated three different types of transgenic animals in which the wild-type copy of *lin-14* was selectively expressed only in PLM, in the hypodermis, or in the body wall muscles, in *lin-14* mutant animals. Interestingly, we found that expression of wild-type *lin-14* in any of these tissues could significantly rescue the axonal degeneration defect of *lin-14* mutants (Figures 3A–3C). Remarkably, expression in the muscle and hypodermis also rescued the other associated phenotypes of axonal misguidance and missing synaptic branches. These results indicate that LIN-14 functions in multiple tissues and that the full penetrance of axonal degeneration is only achieved when this molecule is simultaneously lacking in more than one tissue. To further investigate the mechanism of rescue in these strains, we performed confocal optical cross-sections with the basal lamina marker as described earlier. All three rescue strains displayed an improvement in the embedment of PLM (Figures 3D–3F), with muscle-specific expression providing the most significant rescue. This suggests that the muscle is the main tissue in which LIN-14 is acting to promote embedment. It should also be noted that the lack of embedment by itself is not sufficient to cause a degeneration phenotype (Emtage et al., 2004); rather, the embedment is one highly visible aspect of the miscommunication that occurs in *lin-14* mutants between the axon and its surrounding tissue.

LIN-14 Functions Early in Development to Prevent Axonal Degeneration Later in Life

Previous studies have shown that LIN-14 expression is highest during the L1 stage (Arasu et al., 1991; Ruvkun and Giusto, 1989), suggesting that it functions early in development. Indeed, many of the neuronal functions attributed to LIN-14 are L1-stage specific (Aurelio et al., 2003; Hallam and Jin, 1998; Zou et al., 2012). In contrast, in our phenotypic analysis, the appearance of an axonal degeneration phenotype in PLM during later larval stages hints at a subsequent role for LIN-14 function. In order to determine when LIN-14 is required to regulate the PLM axon, we exploited the temperature-sensitive nature of the *lin-14(n355n679)* allele (Ambros and Horvitz, 1987) and performed a series of temperature-shift experiments. First, as predicted, culturing *lin-14(n355n679)* animals at the permissive temperature (15°C) almost completely abolished the PLM axonal break phenotype observed when the animals were cultured at the restrictive temperature (25°C) (Figure 4A). We then performed shift-down experiments, whereby animals were raised at the restrictive temperature for various periods of time before being transferred to the permissive temperature and analyzed at the L4 stage. In agreement with previous results demonstrating that LIN-14 is expressed early at the L1 stage (Arasu et al., 1991; Ruvkun and Giusto, 1989), we found that animals shifted to the permissive temperature immediately after hatching were largely wild-type in appearance and similar to animals cultured continuously at the permissive temperature (Figure 4B, first and second bars). However, if the shift occurred 1 hr after hatching, the animals presented an axonal break phenotype similar to that observed when they were cultured continuously at the restrictive temperature (Figure 4B, third bar). These data demonstrate that, rather than functioning as a survival factor that is constantly required throughout the organism's life, LIN-14 is

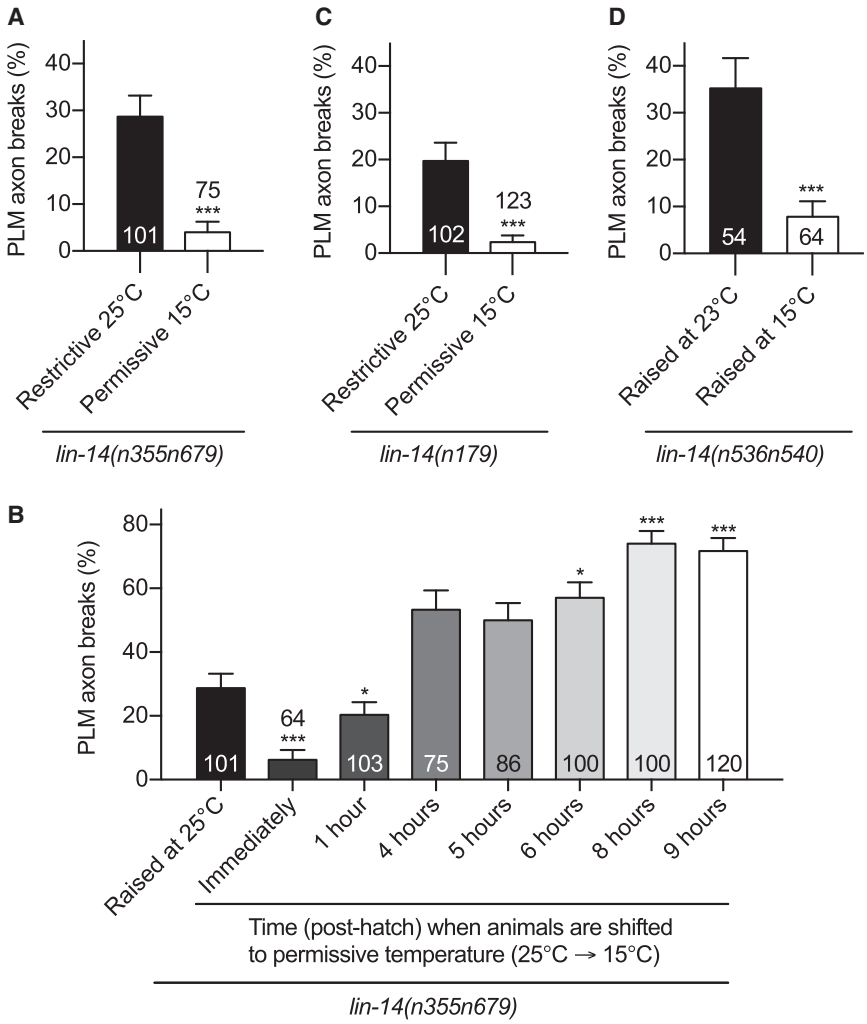

Figure 4. LIN-14 Is Required Early in Development to Maintain the Axonal Structure

(A) *lin-14(n355n679)* animals grown at a restrictive temperature (25°C) and a permissive temperature (15°C).

(B) *lin-14(n355n679)* animals transferred from the restrictive to permissive temperature at various times after hatching, compared to those raised entirely at the restrictive or permissive temperature. Animals transferred from restrictive to permissive conditions immediately after hatching show a significant decrease in axonal breaks at the L4 stage, compared to those raised in restrictive conditions their whole lives. After ≥4 hr of restrictive growth, there is a significant increase in breaks, compared to the number in animals raised solely in restrictive conditions.

(C) *lin-14(n179)* animals grown at the restrictive temperature (25°C) and the permissive temperature (15°C).

(D) *lin-14(n536n540)* mutants raised at 23°C or 15°C. *lin-14(n536n540)* is not known to be a temperature-sensitive mutant; the increase in axonal break with higher temperature, therefore, indicates that the axonal break phenotype in itself is temperature sensitive.

Error bars represent the SE of proportion; n values are indicated at the base of each graph. *$p < 0.05$; ***$p < 0.001$, from the Student's t test for (A), (C), and (D) and from ANOVA and Dunnett's multiple comparison test for (B) (compared to raised at 25°C).

crucial very early in larval development to ensure that axonal integrity is maintained later in life. However, unexpectedly, we found a strong increase in the penetrance of axonal breaks when animals were shifted to permissive conditions at later time points of the L1 stage; this defect was much worse than that of animals raised continuously at the restrictive temperature, reaching 70% when the animals were shifted to the permissive temperature at the very end of L1 (Figure 4B, bars 4 to 8). Importantly, the same temperature-shift paradigms did not cause any axonal-break phenotype in wild-type control animals (*zdIs5*; data not shown), indicating that this enhancement occurred specifically in *lin-14* mutant animals. These data could be explained if the altered heterochronic function of *lin-14* creates a mismatch between the growing rate of different tissues, such as the PLM axon and its surrounding tissue, which could be enhanced by temperature shifts that are well known to affect the rate of body growth. Warmer temperatures up to 25°C cause *C. elegans* to develop almost twice as fast as when they are grown at 15°C (Byerly et al., 1976); thus, shifting animals between different conditions may impact their physical growth and result in mechanical stresses that exacerbate any underlying axon weakness (Tang-Schomer et al., 2010). If this were the case, the temperature-sensitive effect should be extended to other *lin-14* alleles that are not temperature sensitive. Indeed, we found that the axonal-break phenotype was temperature sensitive in the severe allele *lin-14(n536n540)*, in addition to the known temperature-sensitive alleles *lin-14(n179)* and *lin-14(n355n679)* (Figures 4A, 4C, and 4D). These data again support the notion that the tissues surrounding the PLM axon play a major role in maintaining its structure.

Mutations in LIN-14 Cause Axonal Damage through a Two-Hit Effect

The results of the temperature-shift assay (Figure 4), combined with the defect in PLM axonal embedment of *lin-14* animals (Figure 2) and the function of LIN-14 within PLM as well as in the surrounding tissues (Figure 3), have two major implications. First, a key element for the maintenance of PLM axonal integrity is its correct positioning and interaction with its surrounding tissue. Second, disruption of LIN-14 causes axonal damage by simultaneously affecting the PLM axon and its surrounding tissue. Therefore, further disruption of either cytoskeletal elements within the PLM axon, or the interaction between the PLM axon and its surrounding tissue, should cause an increase in axonal degeneration in the *lin-14* mutants. We directly tested this hypothesis by targeting several molecules that are known to affect

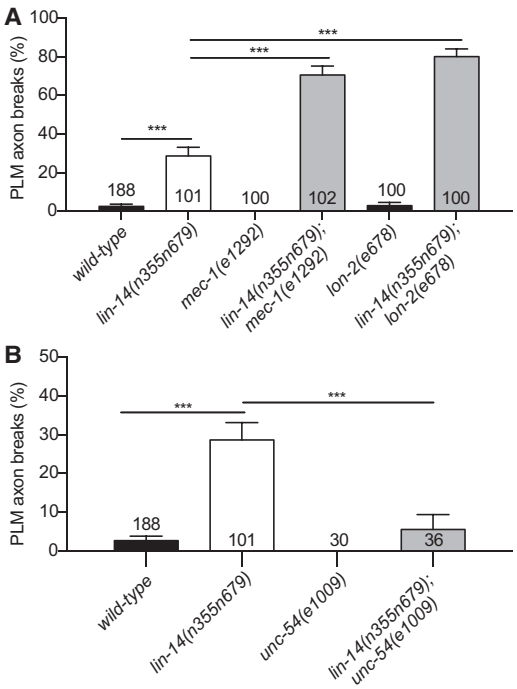

Figure 5. Synergic Interaction of LIN-14 with Molecules that Affect the Surrounding Tissues in Regulating PLM Axonal Maintenance

(A) MEC-1 is required for the correct attachment of the mechanosensory neurons to the body wall, and when mutated in combination with *lin-14 (lin-14; mec-1)*, it causes an increase in the penetrance of PLM axonal breaks. Mutation in the *lon-2* gene causes animals to grow to 50% longer than their wild-type counterparts, but this alone is not sufficient to induce a significant level of breaks in the PLM axon. Double mutants of *lin-14* and *lon-2,* however, show a marked increase in the level of axonal breaks compared to *lin-14* and *lon-2* single mutants.

(B) The *unc-54* gene encodes for the myosin heavy chain protein and is required for locomotion. Mutation of *unc-54* in combination with *lin-14* causes a suppression of the number of axonal breaks in PLM.

Error bars represent SE of proportion; n values are indicated at the base of each graph. ***p < 0.001, from ANOVA and Sidak's multiple comparison test.

these processes. MEC-1 is a protein with multiple disulphyde-linked epidermal growth factor (EGF) and Kunitz domains, which are required for correct attachment of the mechanosensory neurons to the hypodermis (Emtage et al., 2004). Our results revealed that mutation of *mec-1* greatly increased PLM axonal degeneration in *lin-14* mutants (Figure 5A). Importantly, *mec-1* single mutants did not present any axonal degeneration (Figure 5A). Furthermore, we tested whether highly increased body length could enhance the strain placed on the PLM axon in *lin-14* mutants. We predicted that, because PLM is not correctly embedded in the hypodermis in *lin-14* mutants, increasing body length (and, therefore, the length of the PLM axon) would exacerbate the rate of axon breaks. We analyzed animals carrying a mutation in the *lon-2* gene, which causes animals to grow approximately 50% longer than normal (Gumienny et al., 2007). This consistently produced a very large synergistic effect, with more than 80% of animals displaying axonal degeneration in PLM (Figure 5A).

We next investigated the possibility that this synergistic effect may be modulated by alterations in axonal transport and/or mitochondrial number. We tested for aberrations in axonal transport by studying the movement and localization of a fluorescently tagged version of UNC-104/KIF1A, a major kinesin motor molecule. In *lin-14* mutants, UNC-104 was distributed to the distal portion of the axon in a pattern similar to that observed in the wild-type, with 100% of mutant axons displaying accumulation in the distal section (n = 106). The number and distribution of mitochondria were visualized using an mRFP-tagged version of the translocase of outer mitochondrial membrane 20 protein (TOMM-20) (Neumann and Hilliard, 2014). We observed no difference in mitochondrial number or distribution between *lin-14* mutants and wild-type animals: wild-type, 10.2 mitochondria per axon ± 0.8 (SE of proportion; n = 42); *lin-14(n355n679)*, 9.1 mitochondria per axon ± 0.8 (SE of proportion; n = 66); p = 0.259, paired t test. Finally, we tested whether reducing the stress placed on the PLM axon by normal animal movement could rescue the axonal degeneration phenotypes. Indeed, *lin-14* mutant animals that were paralyzed due to a lack of the myosin heavy chain encoded by *unc-54* displayed almost-complete rescue of the axonal degeneration defect (Figure 5B). Thus, the position of the axon within the epidermis, axonal length, and mechanical stress have synergic effects that can affect the capacity of the axon to remain intact.

We then specifically tested whether disrupting the PLM axon itself, rather than the surrounding tissue or entire animal, also enhanced the axonal-break phenotype observed due to the reduction-of-function *lin-14* alleles. Our previous work has shown that animals lacking the α-tubulin acetyltransferase MEC-17, which is expressed exclusively in the mechanosensory neurons, present adult-onset axonal degeneration in PLM neurons due to the loss of microtubule stability (Neumann and Hilliard, 2014). We found that mutation of *mec-17* in combination with *lin-14* significantly increased the axonal degeneration defect of *lin-14* single mutants (Figure 6A). This result reveals a synergistic effect between *mec-17* and *lin-14* and suggests that loss of *lin-14* combined with disruption of microtubule stability enhances the penetrance of axonal degeneration. To examine this further, we treated *lin-14* mutants with microtubule-destabilizing or -stabilizing compounds. Mild destabilization with colchicine caused a large enhancement in the phenotype, whereas stabilization with paclitaxel led to the suppression of axonal degeneration (Figure 6B). These data highlight the importance of microtubule stability for axonal maintenance and establish the role of a functional LIN-14 protein for restricting the levels of axonal degeneration that occur when this structure is disrupted. Taken together, these results reveal that axonal maintenance is regulated by cell-autonomous and non-cell-autonomous factors and that the highest frequency of axonal breaks is caused when multiple components that participate in this process are altered.

To determine whether the apoptosis machinery was important for the observed degeneration, we next investigated the apoptosis-associated molecules CED-4/APAF-1 and the executer caspase CED-3. We found that *ced-4;lin-14* double mutants were indistinguishable from *lin-14* single mutants and did not rescue the axonal degeneration phenotype (Figure S5).

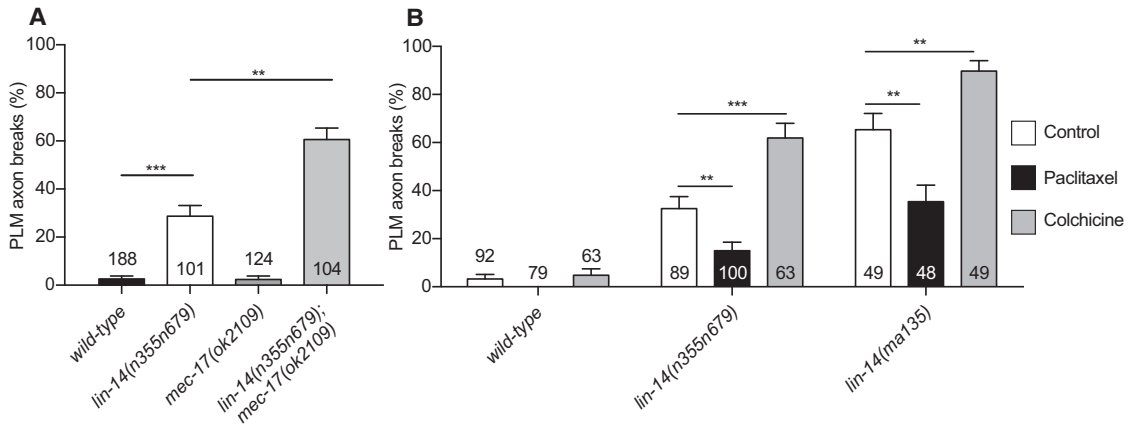

Figure 6. Synergic Interaction of LIN-14 with MEC-17 and Microtubule-Destabilizing Drugs in Regulating PLM Axonal Maintenance

(A) Double mutants of *lin-14* with *mec-17* display a highly increased penetrance of axon breaks. Note that animals were analyzed at the L4 stage, which is prior to the onset of axonal degeneration in the *mec-17* mutants (Neumann and Hilliard, 2014).

(B) Treatment with the microtubule-destabilizing drug colchicine greatly increases the *lin-14* axon breaks, whereas treatment with the microtubule-stabilizing drug paclitaxel rescues this defect. Drug treatments were performed in both the *n355n679* and *ma135* alleles.

Error bars represent SE of proportion; n values are indicated at the base of each graph. $^{**}p < 0.01$; $^{***}p < 0.001$, from ANOVA and Sidak's multiple comparison test for (A) and Dunnett's multiple comparison test for (B) (each group was compared to the specific control).

This indicates that the main apoptotic pathway is not involved in this type of degeneration. Interestingly, a partial rescue of the axonal-break phenotype was observed in the *ced-3;lin-14* double mutants. CED-3, along with some of its target proteins, has previously been shown to have specific roles during development that are entirely distinct from its role in apoptosis (Weaver et al., 2014). One of these targets is LIN-14. Thus, our results confirm the observations of Weaver et al. (2014) and suggest that CED-3 also has a non-apoptotic role in the maintenance of axonal structure.

We were also interested in whether the Wallerian degeneration slow (WLD^S) protein, which has been shown to have a protective effect in other species (Adalbert et al., 2005; Avery et al., 2009; Ferri et al., 2003; Hoopfer et al., 2006; MacDonald et al., 2006; Mack et al., 2001; Martin et al., 2010; Samsam et al., 2003), could prevent axonal degeneration in a *lin-14* mutant background. We did not detect any significant protective effect, indicating that this type of degeneration is different from Wallerian degeneration (Figure S6). This result is supported by our previous work showing that the axonal degeneration process following axotomy in *C. elegans* can proceed independently of the WLD^S and Nmnat pathway (Nichols et al., 2016).

We next investigated the interaction between LIN-14 and the DLK-1 pathway, which has been shown to be a key axonal degeneration-promoting pathway after injury in both mice and *Drosophila* (Miller et al., 2009). DLK-1 is a dual-leucine zipper kinase MAPKKK that has previously been implicated in synaptogenesis, axon outgrowth, and axonal regeneration in *C. elegans* and other species (Byrne et al., 2014; Collins et al., 2006; Hammarlund et al., 2009; Itoh et al., 2009; Lewcock et al., 2007; Nakata et al., 2005; Shin et al., 2012; Watkins et al., 2013; Xiong et al., 2010; Yan et al., 2009). We tested whether lack of *dlk-1* had any effect on the PLM axons of *lin-14* mutant animals. Remarkably, we found that *lin-14;dlk-1* double mutants had a significantly enhanced PLM axonal degeneration phenotype compared to *lin-14* single mutants (*dlk-1* single mutants did not present any axonal degeneration) (Figure 7), indicating a synergistic effect of DLK-1 with LIN-14. DLK-1 levels are regulated by RPM-1, an E3 ligase that targets DLK-1 for degradation (Abrams et al., 2008; Nakata et al., 2005). Thus, absence of RPM-1 would be expected to increase the level of DLK-1. Consistent with this notion, and with the synergistic effect between the DLK-1 pathway and LIN-14, we found that mutations in *rpm-1* rescued the *lin-14* axonal degeneration defects (Figure 7). These results provide evidence of a strong synergy between *lin-14* and the *dlk-1/rpm-1* pathway and demonstrate that this pathway can robustly modulate the rate of axonal degeneration caused by disruption of LIN-14 function.

Finally, as the DLK-1 pathway has previously been shown to be a major mediator of axonal degeneration after injury in other species, we asked whether LIN-14 plays a similar function. We performed axotomy on PLM and scored the rate of axonal clearance of the distal fragment in *lin-14* animals, compared to wild-type controls (Figure S7). We focused on the L1 and L4 stages, as we have shown that these are the most critical for this process (Nichols et al., 2016). We found no significant difference between *lin-14* and wild-type animals (Figure S7). This is consistent with our previous finding that DLK-1 does not modulate injury-induced axonal degeneration in *C. elegans* (Nichols et al., 2016). These results indicate that LIN-14 has a specific role in protecting the axon from spontaneous degeneration rather than from the self-destruction and clearance process initiated by transection injuries.

In conclusion, our data support a model in which the heterochronic molecule LIN-14 functions both inside and outside the neuron to regulate the maintenance of the axon. The absence or altered expression of LIN-14 early in life causes

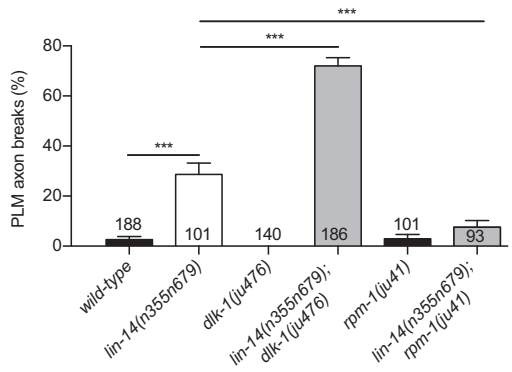

Figure 7. Synergic Interaction of LIN-14 with DLK-1 in Regulating PLM Axonal Maintenance

Double mutants of *lin-14* with *dlk-1* result in an increased penetrance of axonal breaks. Conversely, double mutants with *rpm-1*, which functions to reduce *dlk-1* levels, exhibit a decrease in PLM axon breaks. Error bars represent SE of proportion; n values are indicated at the base of each graph. ***$p < 0.001$, from ANOVA and Sidak's multiple comparison test.

long-lasting effects that only become apparent as the animal ages. This form of predetermined deleterious degeneration could be the mediator of a number of neurodegenerative conditions and could, therefore, offer opportunities to intervene before the phenotypes and damage fully manifest.

EXPERIMENTAL PROCEDURES

Strains

All nematodes were cultured under standard conditions (Brenner, 1974). Unless noted otherwise, experiments were performed on L4-stage hermaphrodites raised at 25°C. The wild-type Bristol N2 strain and the following mutations were used: *lin-14(n179)*; *lin-14(n355n679)*; *lin-14(n536n540)*; *lin-14 (ma135)*; *lin-14(n727)*; *dgn-1(cg121)*; *unc-53(e2432)*; *mec-1(e1292)*; *lon-2 (e678)*; *unc-54(e1009)*; *mec-17(ok2109)*; *ced-4(n1162)*; *ced-3(n717)*; *dlk-1 (ju476)*; and *rpm-1(ju41)*.

The transgenes used were: *zdIs5(Pmec-4::GFP)*; *qyIs127(plam-1::lam-1:: mCherry + unc-119(+))*; *vdEx907(5 ng/μL Pmec-4::lin-14 + Podr-1::DsRed)*; *vdEx1260(5 ng/μL Pmyo-3::lin-14 + Podr-1::DsRed)*; *vdEx1354(5 ng/μL Pdpy-7::lin-14 + Podr-1::DsRed)*; *juIs76(Punc-25::GFP)*; *zaIs2(lin-14::GFP + rol-6 (su1006))*; *vdEx263(Pmec-4::mCherry + Podr-1::DsRed)*; *jsIs1111 (Pmec-4::UNC-104::GFP)*; *vdEx484(0.5 ng/μL Pmec-4::tomm-20::mRFP + Punc-122::GFP)*; *and vdEx295(10 ng/μL Pmec-4::WLD^S + Podr-1::DsRed)*.

Phenotypic Analyses

Unless otherwise specified, PLM morphology was analyzed in L4-stage animals in a *zdIs5*(*Pmec-4::GFP*) background. Developmental analyses were performed in synchronized populations of hatched animals by collecting newly hatched nematodes from plates containing only eggs. Temperature-shift experiments were conducted by growing animals at 25°C for at least two generations before synchronous populations were obtained by hatch-off. Animals were subsequently allowed to remain at 25°C for defined times after hatching (1, 4, or ≥5 hr) before being shifted for growth at 15°C until the L4 stage, when axon morphology was examined.

Molecular Biology

Molecular biology was performed using standard techniques (Sambrook et al., 1989). Construction of the *Pmec-4::lin-14*, *Pmyo-3::lin-14*, and *Pdpy-7::lin-14* plasmids was conducted using the pSM plasmid backbone and Gibson cloning (Gibson et al., 2009) of amplified *lin-14* sequences from the pB14RGFP and pVT3333dg plasmids (Hong et al., 2000), both kindly provided by Victor Ambros (University of Massachusetts Medical School, Worcester, MA, USA). PCR for genotyping used Phusion or Taq DNA Polymerase sourced from New England Biolabs, with genomic DNA templates obtained from whole animal lysates (Wicks et al., 2001). All primers were sourced from GeneWorks (Adelaide, Australia). Plasmids were transformed into *E. coli* (strain DH5α) and purified using the QIAprep Spin Miniprep Kit (QIAGEN). DNA sequencing of each construct was performed by the Australian Genome Research Facility (Brisbane, Australia).

Microscopy

Animals were inspected by mounting on 4% agar pads after anesthesia with 0.03% tetramisole hydrochloride. Fluorescence microscopy was performed using upright Zeiss AxioImager Z1 and Zeiss AxioImager A1 microscopes equipped with a Photometrics Cool Snap HQ^2 camera. Images acquired in Metamorph software were further processed in ImageJ and Adobe Photoshop CS5. YZ-plane confocal optical cross-sections were generated by using confocal z stack images performed with a spinning-disk confocal microscope (Yokogawa), followed by using the YZ-plane orthogonal views function in ImageJ. All spinning-disk confocal microscopy images were deconvolved with Huygens Professional, v.16.05 (Scientific Volume Imaging, the Netherlands) using the CMLE algorithm, with signal to noise ratio (SNR):20 and 40 iterations. Microinjections were performed using standard methods (Mello et al., 1991), with an inverted Zeiss AxioObserver microscope equipped with differential interference contrast, a Narishige needle holder, and an Eppendorf FemtoJet pump.

Drug Treatment

Animals were grown on nematode growth medium (NGM) agar plates containing 0.1 mM colchicine (Sigma-Aldrich) or 1 μM paclitaxel (Sigma-Aldrich) in DMSO as previously described (Chalfie and Thomson, 1982; Kirszenblat et al., 2013; Neumann and Hilliard, 2014). For control plates, animals were grown with 1% DMSO. Parental (P0) animals were grown from the L4 stage on drug plates, and their F1 progeny were scored.

Laser Axotomy

Laser axotomies were performed as we have previously described (Neumann et al., 2011), using a MicroPoint Laser System Basic Unit attached to a Zeiss Axio Imager A1 (Objective EC Plan-Neofluar 100×/1.30 Oil M27). This laser delivers 120 mJ of 337 nm energy with a 2- to 6-ns pulse length. Axotomies were completed with 10 to 20 pulses in both wild-type and *lin-14(n355n679)* mutant animals. The PLM axon of animals at the L4 stage was cut at a point approximately 50 μm anterior to the PLM cell body, and the resulting distal fragment was assessed for degeneration 72 hr post-axotomy. The PLM axon of animals at the L1 stage was cut approximately 10 μm from the cell body and analyzed 16 hr post-axotomy. *lin-14(n355n679)* mutants that already displayed axonal degeneration and breaks before being axotomized were excluded from these experiments. Neurons that underwent post-axotomy axonal fusion were also excluded. The severity of degeneration and clearance was analyzed for each neuron using an arbitrary scale (1 = fully cleared axon, 2 = multiple breaks, 3 = one break, 4 = beading and thinning, and 5 = intact axon) (Nichols et al., 2016).

Statistical Analyses

GraphPad Prism was used for statistical analyses. Error of proportions was used to estimate variation within a single population. We used the Student's t test or Mann-Whitney for pairwise comparisons, whereas ANOVA Sidak's, Dunnett's, or Tukey's multiple comparisons tests were used as indicated in each figure.

SUPPLEMENTAL INFORMATION

Supplemental Information includes seven figures and can be found with this article online at http://dx.doi.org/10.1016/j.celrep.2017.08.083.

AUTHOR CONTRIBUTIONS

F.K.R., R.K., and J.C. carried out most experiments. R.G. and M.G. contributed some experiments. F.K.R., R.K., J.C., M.A.H., B.N., and M.G. designed and interpreted experiments and wrote and edited the paper.

ACKNOWLEDGMENTS

We thank Sean Coakley for providing invaluable help with the cross-section imaging; Rowan Tweedale for comments on the manuscript; members of the Hilliard lab for valuable discussions and comments; Luke Hammond, Arthur Chien, and Rumelo Amor for support with microscopy; and Nick Valmas for support with graphic design. Some strains were provided by the *Caenorhabditis* Genetics Center (CGC), which is funded by the NIH Office of Research Infrastructure Programs (P40 OD010440), and the International *C. elegans* Gene Knockout Consortium. This work was supported by NHMRC project grant 631634, NIH grant R01 NS060129, an ARC Future Fellowship (FT110100097), and an NHMRC Senior Research Fellowship (1111042) to M.A.H.; an NHMRC project grant (1099690) to B.N.; and a University of Queensland Research Scholarship (UQRS) to J.C. Imaging was performed at the Queensland Brain Institute's Advanced Microscopy Facility. An ARC LIEF grant (LE130100078) funded the microscopy equipment.

Received: March 17, 2017
Revised: July 31, 2017
Accepted: August 25, 2017
Published: September 19, 2017

REFERENCES

Abrams, B., Grill, B., Huang, X., and Jin, Y. (2008). Cellular and molecular determinants targeting the *Caenorhabditis elegans* PHR protein RPM-1 to perisynaptic regions. Dev. Dyn. *237*, 630–639.

Adalbert, R., Gillingwater, T.H., Haley, J.E., Bridge, K., Beirowski, B., Berek, L., Wagner, D., Grumme, D., Thomson, D., Celik, A., et al. (2005). A rat model of slow Wallerian degeneration (WldS) with improved preservation of neuromuscular synapses. Eur. J. Neurosci. *21*, 271–277.

Ambros, V., and Horvitz, H.R. (1984). Heterochronic mutants of the nematode *Caenorhabditis elegans*. Science *226*, 409–416.

Ambros, V., and Horvitz, H.R. (1987). The *lin-14* locus of *Caenorhabditis elegans* controls the time of expression of specific postembryonic developmental events. Genes Dev. *1*, 398–414.

Arasu, P., Wightman, B., and Ruvkun, G. (1991). Temporal regulation of *lin-14* by the antagonistic action of two other heterochronic genes, *lin-4* and *lin-28*. Genes Dev. *5*, 1825–1833.

Aurelio, O., Boulin, T., and Hobert, O. (2003). Identification of spatial and temporal cues that regulate postembryonic expression of axon maintenance factors in the *C. elegans* ventral nerve cord. Development *130*, 599–610.

Avery, M.A., Sheehan, A.E., Kerr, K.S., Wang, J., and Freeman, M.R. (2009). Wld^S requires Nmnat1 enzymatic activity and N16–VCP interactions to suppress Wallerian degeneration. J. Cell Biol. *184*, 501–513.

Brenner, S. (1974). The genetics of *Caenorhabditis elegans*. Genetics *77*, 71–94.

Byerly, L., Cassada, R.C., and Russell, R.L. (1976). The life cycle of the nematode *Caenorhabditis elegans*. I. Wild-type growth and reproduction. Dev. Biol. *51*, 23–33.

Byrne, A.B., Walradt, T., Gardner, K.E., Hubbert, A., Reinke, V., and Hammarlund, M. (2014). Insulin/IGF1 signaling inhibits age-dependent axon regeneration. Neuron *81*, 561–573.

Chalfie, M., and Thomson, J.N. (1982). Structural and functional diversity in the neuronal microtubules of *Caenorhabditis elegans*. J. Cell Biol. *93*, 15–23.

Chalfie, M., Sulston, J.E., White, J.G., Southgate, E., Thomson, J.N., and Brenner, S. (1985). The neural circuit for touch sensitivity in *Caenorhabditis elegans*. J. Neurosci. *5*, 956–964.

Cifuentes-Diaz, C., Nicole, S., Velasco, M.E., Borra-Cebrian, C., Panozzo, C., Frugier, T., Millet, G., Roblot, N., Joshi, V., and Melki, J. (2002). Neurofilament accumulation at the motor endplate and lack of axonal sprouting in a spinal muscular atrophy mouse model. Hum. Mol. Genet. *11*, 1439–1447.

Coleman, M. (2005). Axon degeneration mechanisms: commonality amid diversity. Nat. Rev. Neurosci. *6*, 889–898.

Collins, C.A., Wairkar, Y.P., Johnson, S.L., and DiAntonio, A. (2006). Highwire restrains synaptic growth by attenuating a MAP kinase signal. Neuron *51*, 57–69.

Conforti, L., Adalbert, R., and Coleman, M.P. (2007). Neuronal death: where does the end begin? Trends Neurosci. *30*, 159–166.

Emtage, L., Gu, G., Hartwieg, E., and Chalfie, M. (2004). Extracellular proteins organize the mechanosensory channel complex in *C. elegans* touch receptor neurons. Neuron *44*, 795–807.

Ferri, A., Sanes, J.R., Coleman, M.P., Cunningham, J.M., and Kato, A.C. (2003). Inhibiting axon degeneration and synapse loss attenuates apoptosis and disease progression in a mouse model of motoneuron disease. Curr. Biol. *13*, 669–673.

Fischer, L.R., Culver, D.G., Davis, A.A., Tennant, P., Wang, M., Coleman, M., Asress, S., Adalbert, R., Alexander, G.M., and Glass, J.D. (2005). The Wld^S gene modestly prolongs survival in the $SOD1^{G93A}$ fALS mouse. Neurobiol. Dis. *19*, 293–300.

Gallegos, M.E., and Bargmann, C.I. (2004). Mechanosensory neurite termination and tiling depend on SAX-2 and the SAX-1 kinase. Neuron *44*, 239–249.

Gibson, D.G., Young, L., Chuang, R.Y., Venter, J.C., Hutchison, C.A., 3rd, and Smith, H.O. (2009). Enzymatic assembly of DNA molecules up to several hundred kilobases. Nat. Methods *6*, 343–345.

Gumienny, T.L., MacNeil, L.T., Wang, H., de Bono, M., Wrana, J.L., and Padgett, R.W. (2007). Glypican LON-2 is a conserved negative regulator of BMP-like signaling in *Caenorhabditis elegans*. Curr. Biol. *17*, 159–164.

Hallam, S.J., and Jin, Y. (1998). *lin-14* regulates the timing of synaptic remodelling in *Caenorhabditis elegans*. Nature *395*, 78–82.

Hammarlund, M., Jorgensen, E.M., and Bastiani, M.J. (2007). Axons break in animals lacking beta-spectrin. J. Cell Biol. *176*, 269–275.

Hammarlund, M., Nix, P., Hauth, L., Jorgensen, E.M., and Bastiani, M. (2009). Axon regeneration requires a conserved MAP kinase pathway. Science *323*, 802–806.

Hekimi, S., and Kershaw, D. (1993). Axonal guidance defects in a *Caenorhabditis elegans* mutant reveal cell-extrinsic determinants of neuronal morphology. J. Neurosci. *13*, 4254–4271.

Hong, Y., Lee, R.C., and Ambros, V. (2000). Structure and function analysis of LIN-14, a temporal regulator of postembryonic developmental events in *Caenorhabditis elegans*. Mol. Cell. Biol. *20*, 2285–2295.

Hoopfer, E.D., McLaughlin, T., Watts, R.J., Schuldiner, O., O'Leary, D.D., and Luo, L. (2006). Wld^S protection distinguishes axon degeneration following injury from naturally occurring developmental pruning. Neuron *50*, 883–895.

Hristova, M., Birse, D., Hong, Y., and Ambros, V. (2005). The *Caenorhabditis elegans* heterochronic regulator LIN-14 is a novel transcription factor that controls the developmental timing of transcription from the insulin/insulin-like growth factor gene *ins-33* by direct DNA binding. Mol. Cell. Biol. *25*, 11059–11072.

Itoh, A., Horiuchi, M., Bannerman, P., Pleasure, D., and Itoh, T. (2009). Impaired regenerative response of primary sensory neurons in ZPK/DLK gene-trap mice. Biochem. Biophys. Res. Commun. *383*, 258–262.

Johnson, R.P., and Kramer, J.M. (2012). *C. elegans* dystroglycan coordinates responsiveness of follower axons to dorsal/ventral and anterior/posterior guidance cues. Dev. Neurobiol. *72*, 1498–1515.

Kirszenblat, L., Neumann, B., Coakley, S., and Hilliard, M.A. (2013). A dominant mutation in mec-7/β-tubulin affects exon development and regeneration in *Caenorhabditis elegans* neurons. Mol. Cell. Biol. *24*, 285–296.

Lewcock, J.W., Genoud, N., Lettieri, K., and Pfaff, S.L. (2007). The ubiquitin ligase Phr1 regulates axon outgrowth through modulation of microtubule dynamics. Neuron *56*, 604–620.

MacDonald, J.M., Beach, M.G., Porpiglia, E., Sheehan, A.E., Watts, R.J., and Freeman, M.R. (2006). The *Drosophila* cell corpse engulfment receptor Draper mediates glial clearance of severed axons. Neuron *50*, 869–881.

Mack, T.G., Reiner, M., Beirowski, B., Mi, W., Emanuelli, M., Wagner, D., Thomson, D., Gillingwater, T., Court, F., Conforti, L., et al. (2001). Wallerian

degeneration of injured axons and synapses is delayed by a Ube4b/Nmnat chimeric gene. Nat. Neurosci. *4*, 1199–1206.

Martin, S.M., O'Brien, G.S., Portera-Cailliau, C., and Sagasti, A. (2010). Wallerian degeneration of zebrafish trigeminal axons in the skin is required for regeneration and developmental pruning. Development *137*, 3985–3994.

Mello, C.C., Kramer, J.M., Stinchcomb, D., and Ambros, V. (1991). Efficient gene transfer in *C. elegans*: extrachromosomal maintenance and integration of transforming sequences. EMBO J. *10*, 3959–3970.

Miller, B.R., Press, C., Daniels, R.W., Sasaki, Y., Milbrandt, J., and DiAntonio, A. (2009). A dual leucine kinase-dependent axon self-destruction program promotes Wallerian degeneration. Nat. Neurosci. *12*, 387–389.

Mitani, S., Du, H., Hall, D.H., Driscoll, M., and Chalfie, M. (1993). Combinatorial control of touch receptor neuron expression in *Caenorhabditis elegans*. Development *119*, 773–783.

Nakata, K., Abrams, B., Grill, B., Goncharov, A., Huang, X., Chisholm, A.D., and Jin, Y. (2005). Regulation of a DLK-1 and p38 MAP kinase pathway by the ubiquitin ligase RPM-1 is required for presynaptic development. Cell *120*, 407–420.

Neumann, B., and Hilliard, M.A. (2014). Loss of MEC-17 leads to microtubule instability and axonal degeneration. Cell Rep. *6*, 93–103.

Neumann, B., Nguyen, K.C.Q., Hall, D.H., Ben-Yakar, A., and Hilliard, M.A. (2011). Axonal regeneration proceeds through specific axonal fusion in transected *C. elegans* neurons. Dev. Dyn. *240*, 1365–1372.

Nichols, A.L., Meelkop, E., Linton, C., Giordano-Santini, R., Sullivan, R.K., Donato, A., Nolan, C., Hall, D.H., Xue, D., Neumann, B., et al. (2016). The apoptotic engulfment machinery regulates axonal degeneration in *C. elegans* neurons. Cell Rep. *14*, 1673–1683.

Pan, C.L., Peng, C.Y., Chen, C.H., and McIntire, S. (2011). Genetic analysis of age-dependent defects of the *Caenorhabditis elegans* touch receptor neurons. Proc. Natl. Acad. Sci. USA *108*, 9274–9279.

Raff, M.C., Whitmore, A.V., and Finn, J.T. (2002). Axonal self-destruction and neurodegeneration. Science *296*, 868–871.

Rawson, R.L., Yam, L., Weimer, R.M., Bend, E.G., Hartwieg, E., Horvitz, H.R., Clark, S.G., and Jorgensen, E.M. (2014). Axons degenerate in the absence of mitochondria in *C. elegans*. Curr. Biol. *24*, 760–765.

Reinhart, B.J., and Ruvkun, G. (2001). Isoform-specific mutations in the *Caenorhabditis elegans* heterochronic gene *lin-14* affect stage-specific patterning. Genetics *157*, 199–209.

Ruvkun, G., and Giusto, J. (1989). The *Caenorhabditis elegans* heterochronic gene *lin-14* encodes a nuclear protein that forms a temporal developmental switch. Nature *338*, 313–319.

Sambrook, J., Fritsch, E.F., and Maniatis, T. (1989). Molecular Cloning: A Laboratory Manual (Cold Spring Harbor Laboratory).

Samsam, M., Mi, W., Wessig, C., Zielasek, J., Toyka, K.V., Coleman, M.P., and Martini, R. (2003). The Wld^S mutation delays robust loss of motor and sensory axons in a genetic model for myelin-related axonopathy. J. Neurosci. *23*, 2833–2839.

Schlamp, C.L., Li, Y., Dietz, J.A., Janssen, K.T., and Nickells, R.W. (2006). Progressive ganglion cell loss and optic nerve degeneration in DBA/2J mice is variable and asymmetric. BMC Neurosci. *7*, 66.

Shin, J.E., Cho, Y., Beirowski, B., Milbrandt, J., Cavalli, V., and DiAntonio, A. (2012). Dual leucine zipper kinase is required for retrograde injury signaling and axonal regeneration. Neuron *74*, 1015–1022.

Stokin, G.B., Lillo, C., Falzone, T.L., Brusch, R.G., Rockenstein, E., Mount, S.L., Raman, R., Davies, P., Masliah, E., Williams, D.S., et al. (2005). Axonopathy and transport deficits early in the pathogenesis of Alzheimer's disease. Science *307*, 1282–1288.

Tang-Schomer, M.D., Patel, A.R., Baas, P.W., and Smith, D.H. (2010). Mechanical breaking of microtubules in axons during dynamic stretch injury underlies delayed elasticity, microtubule disassembly, and axon degeneration. FASEB J. *24*, 1401–1410.

Tank, E.M., Rodgers, K.E., and Kenyon, C. (2011). Spontaneous age-related neurite branching in *Caenorhabditis elegans*. J. Neurosci. *31*, 9279–9288.

Toth, M.L., Melentijevic, I., Shah, L., Bhatia, A., Lu, K., Talwar, A., Naji, H., Ibanez-Ventoso, C., Ghose, P., Jevince, A., et al. (2012). Neurite sprouting and synapse deterioration in the aging *Caenorhabditis elegans* nervous system. J. Neurosci. *32*, 8778–8790.

Trapp, B.D., Peterson, J., Ransohoff, R.M., Rudick, R., Mork, S., and Bo, L. (1998). Axonal transection in the lesions of multiple sclerosis. N. Engl. J. Med. *338*, 278–285.

Wang, J.T., Medress, Z.A., and Barres, B.A. (2012). Axon degeneration: molecular mechanisms of a self-destruction pathway. J. Cell Biol. *196*, 7–18.

Watkins, T.A., Wang, B., Huntwork-Rodriguez, S., Yang, J., Jiang, Z., Eastham-Anderson, J., Modrusan, Z., Kaminker, J.S., Tessier-Lavigne, M., and Lewcock, J.W. (2013). DLK initiates a transcriptional program that couples apoptotic and regenerative responses to axonal injury. Proc. Natl. Acad. Sci. USA *110*, 4039–4044.

Weaver, B.P., Zabinsky, R., Weaver, Y.M., Lee, E.S., Xue, D., and Han, M. (2014). CED-3 caspase acts with miRNAs to regulate non-apoptotic gene expression dynamics for robust development in *C. elegans*. eLife *3*, e04265.

Wicks, S.R., Yeh, R.T., Gish, W.R., Waterston, R.H., and Plasterk, R.H.A. (2001). Rapid gene mapping in *Caenorhabditis elegans* using a high density polymorphism map. Nat. Genet. *28*, 160–164.

Wightman, B., Burglin, T.R., Gatto, J., Arasu, P., and Ruvkun, G. (1991). Negative regulatory sequences in the *lin-14* 3′-untranslated region are necessary to generate a temporal switch during *Caenorhabditis elegans* development. Genes Dev. *5*, 1813–1824.

Wightman, B., Ha, I., and Ruvkun, G. (1993). Posttranscriptional regulation of the heterochronic gene *lin-14* by *lin-4* mediates temporal pattern formation in *C. elegans*. Cell *75*, 855–862.

Xiong, X., Wang, X., Ewanek, R., Bhat, P., Diantonio, A., and Collins, C.A. (2010). Protein turnover of the Wallenda/DLK kinase regulates a retrograde response to axonal injury. J. Cell Biol. *191*, 211–223.

Yan, D., Wu, Z., Chisholm, A.D., and Jin, Y. (2009). The DLK-1 kinase promotes mRNA stability and local translation in *C. elegans* synapses and axon regeneration. Cell *138*, 1005–1018.

Zou, Y., Chiu, H., Domenger, D., Chuang, C.F., and Chang, C. (2012). The *lin-4* microRNA targets the LIN-14 transcription factor to inhibit netrin-mediated axon attraction. Sci. Signal. *5*, ra43.

Cell Reports, Volume *20*

Supplemental Information

The Heterochronic Gene *lin-14* Controls Axonal Degeneration in *C. elegans* Neurons

Fiona K. Ritchie, Rhianna Knable, Justin Chaplin, Rhiannon Gursanscky, Maria Gallegos, Brent Neumann, and Massimo A. Hilliard

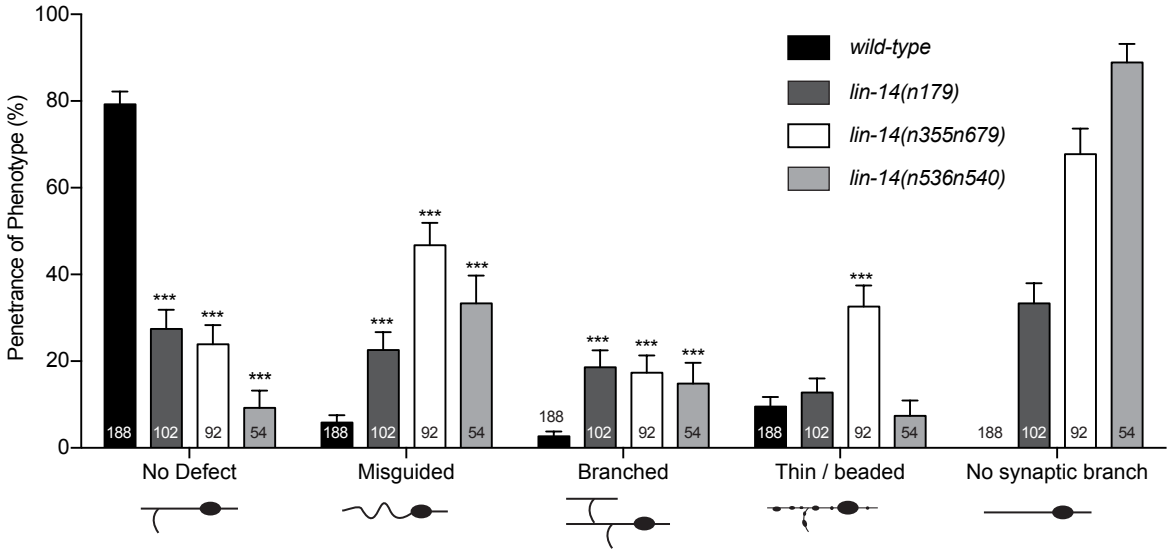

Figure S1. Additional defects of *lin-14* mutant animals in PLM neurons. Related to Figure 1.
Quantification and schemes of additional axonal defects observed in *lin-14* mutant animals for the two PLM neurons. Error bars represent SE of proportion; n represented at the base of each graph, P values from ANOVA Dunnett's multiple comparison test (each group compared to the wild-type); ***p<0.001.

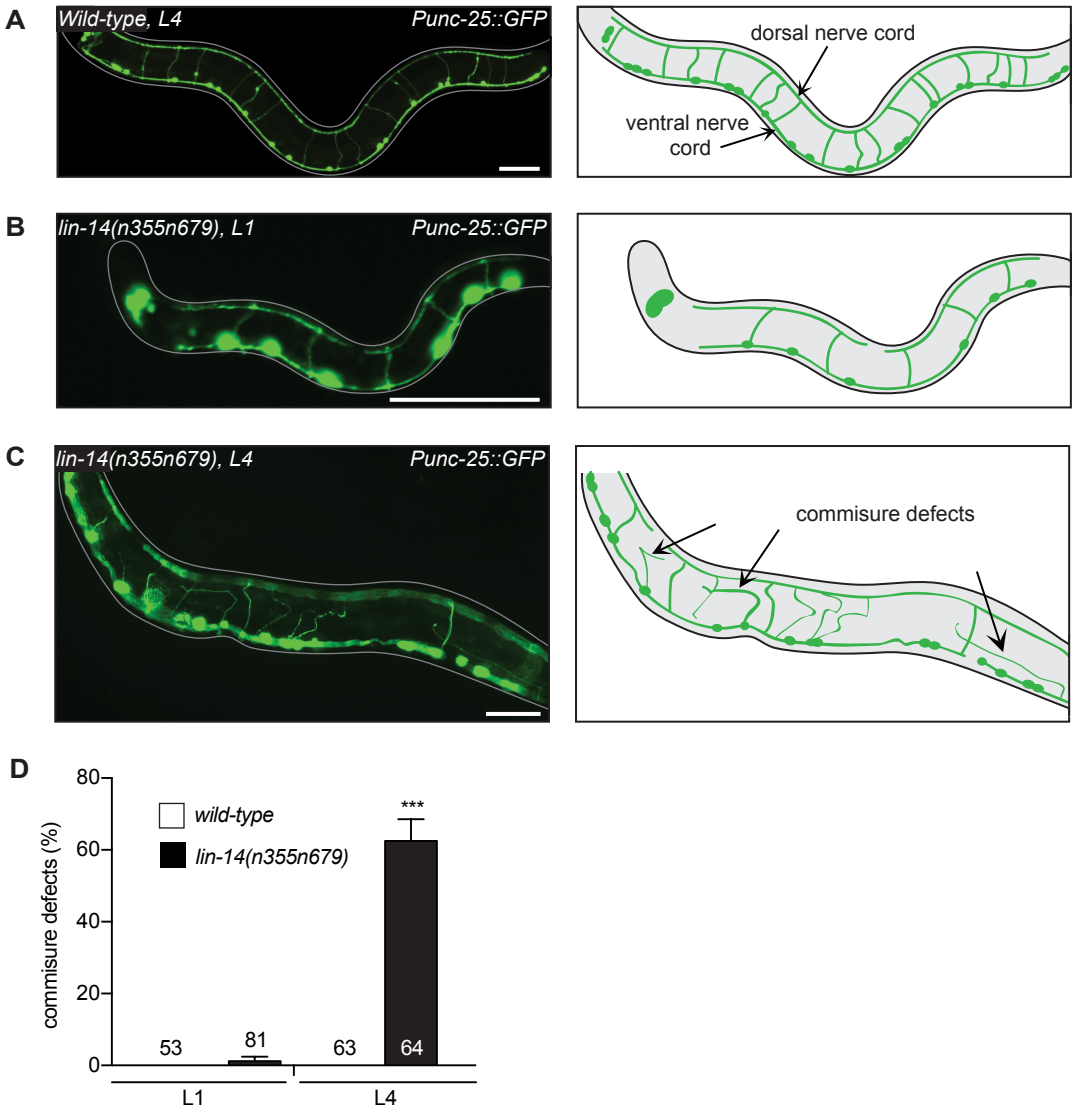

Figure S2. LIN-14 prevents axonal degeneration in the DD/VD motor neurons. Related to Figure 1. (A) Image and schematic of a typical wild-type *juIs76(Punc-25::GFP)* larval stage four (L4) animal, illustrating the DD/VD motor neurons. (B) Image and schematic of a typical L1 *lin-14(n355n679)* mutant animal. (C) Image and schematic of typical commissure defects (arrows) in an L4 *lin-14(n355n679)* mutant animal. (D) Quantification of commissure defects observed in *lin-14* mutant animals for the 19 DD and VD motor neurons in a *juIs76(Punc-25::GFP)* background strain at the L1 and L4 stages. Error bars represent SE of proportion; n represented at the base of each graph; P values from ANOVA Tukey's multiple comparison test; ***p<0.001. Scale bars represent 50 μm.

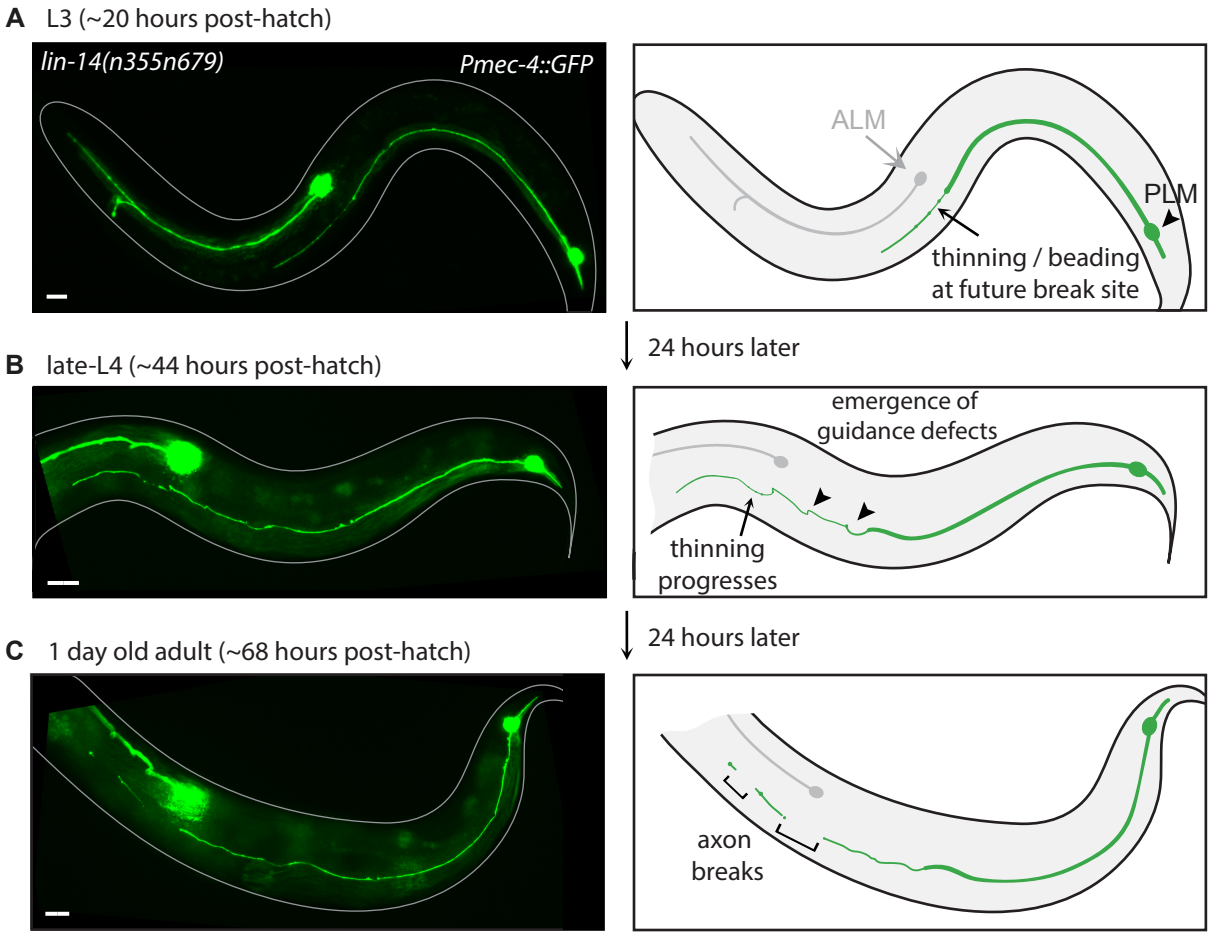

Figure S3. Time-lapse imaging of *lin-14* mutant axonal degeneration. Related to Figure 1.
(A) Image and schematic of a larval stage 3 (L3 ~20 hours post-hatch) *lin-14(n355n679)* mutant animal in a *zdIs5(Pmec-4::GFP)* background. The axon of PLM is guided normally and shows no breaks, though some thinning is evident in the distal portion. (B) Image and schematic of the same animal 24 hours later, now at the L4 stage (~44 hours post-hatch). Guidance defects (in the form of axonal sagging) have started to emerge in addition to the thinning, however no breaks have developed. (C) Image and schematic of the same animal which is now a 1 day old adult (~68 hours post-hatch). Axonal breaks have now appeared in positions where thinning and guidance defects were first observed. Scale bars represent 20 μm.

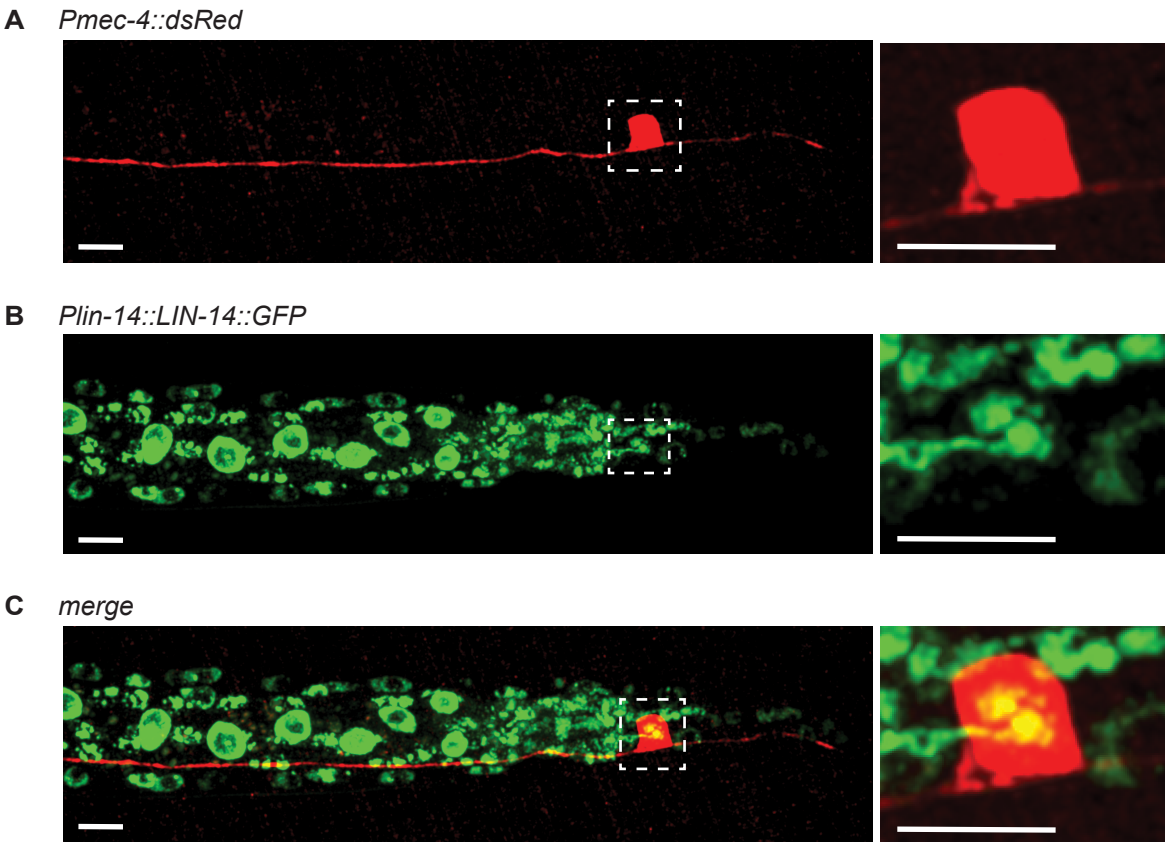

Figure S4. LIN-14 is expressed in PLM neurons. Related to Figure 3.
Confocal images of a L1 stage animal (immediately after hatching). (A) PLM is visualized with mCherry expressed under the *mec-4* promoter. (B) GFP-tagged LIN-14 expressed under the endogenous promoter. (C) A merge of the red and green channels shows that LIN-14 is clearly present in the nucleus of the PLM neuron. Scale bar is 5 μm.

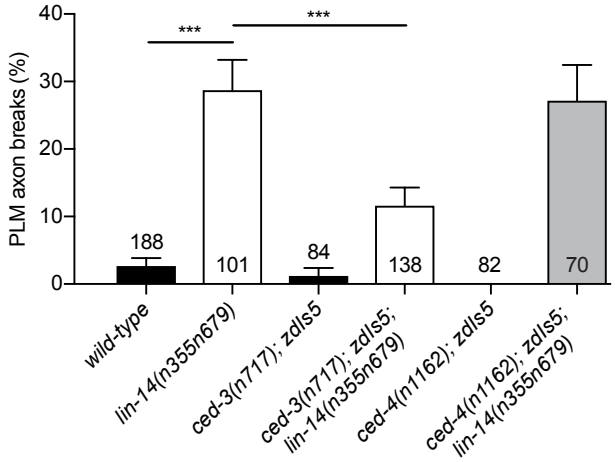

Figure S5. Interaction of LIN-14 with apoptotic molecules CED-4 and CED-3. Related to Figure 5 and 6. Double mutants of *lin-14* with *ced-3* showed a partial rescue of the axonal break phenotype. Conversely, double mutants with *ced-4* had no effect on axonal breaks indicating that the main apoptotic pathway is not involved in this type of degeneration. Error bars represent SE of proportion; n represented at the base of each graph; P values from ANOVA Sidak's multiple comparison test; ***p<0.001.

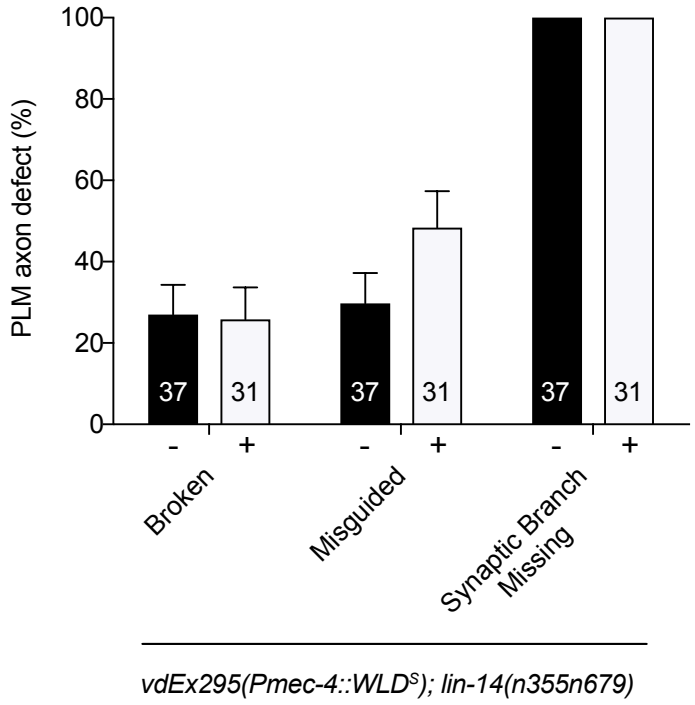

Figure S6. WLD^S does not protect the axon from LIN-14-induced axonal breaks. Related to Figure 5 and 6. *lin-14(n355n679)* mutants carrying the *Pmec-4::WLD^S* transgene (+) present no significant difference in the penetrance of breaks, axon guidance or synaptic branch formation compared to their non-transgenic siblings (-). Error bars represent SE of proportion; n represented at the base of each graph.

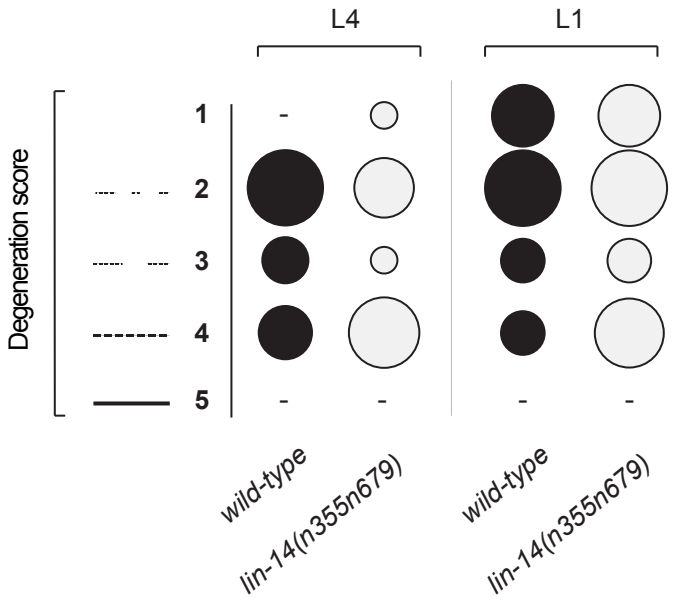

Figure S7. LIN-14 is not involved in axonal clearance following laser-induced transection. Related to Figure 7. Quantification of degeneration of distal fragments in PLM axons that have undergone laser-induced axotomy. The scale of degeneration (y axis) is represented by arbitrary units (1 = fully cleared axon, 2 = multiple breaks, 3 = one break, 4 = beading and thinning, and 5 = intact axon). The area of each circle represents the proportion of animals in each category. n ≥ 14 animals. Mann-Whitney test used for pairwise comparisons.